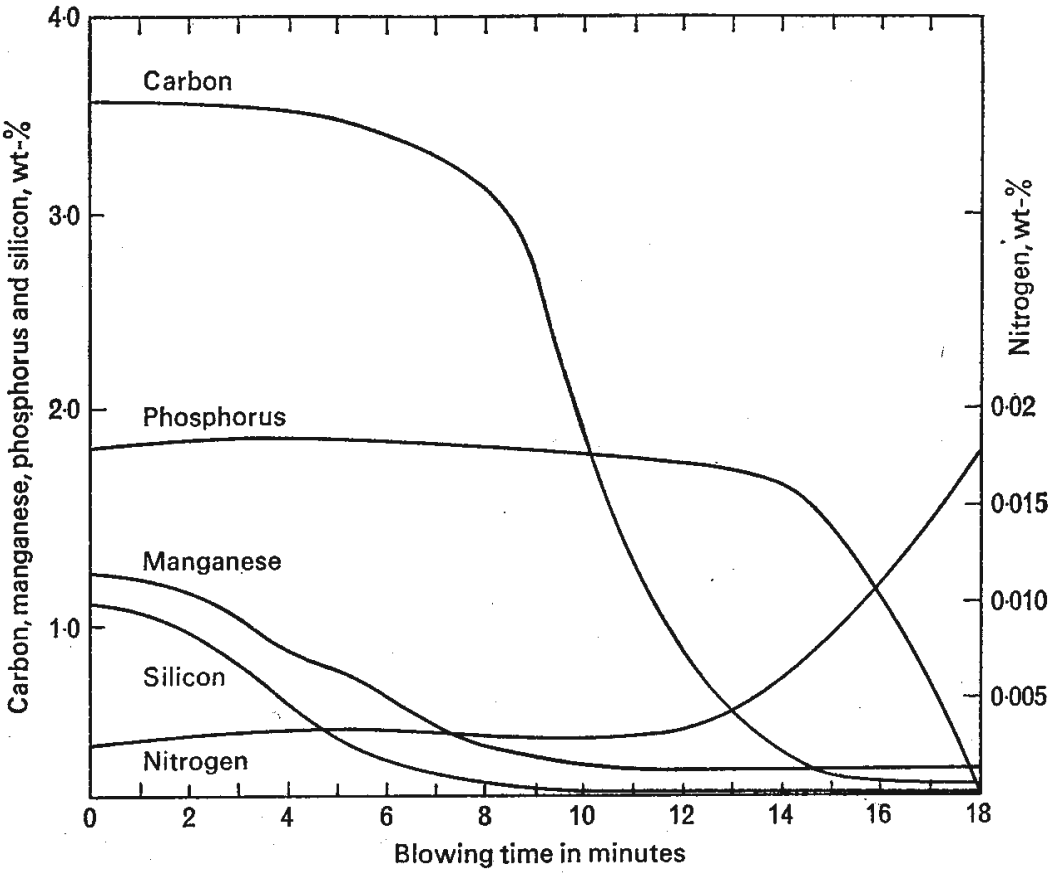

Figure 2.1 Change of metal composition with time in the "Basic Bessemer process"[7]

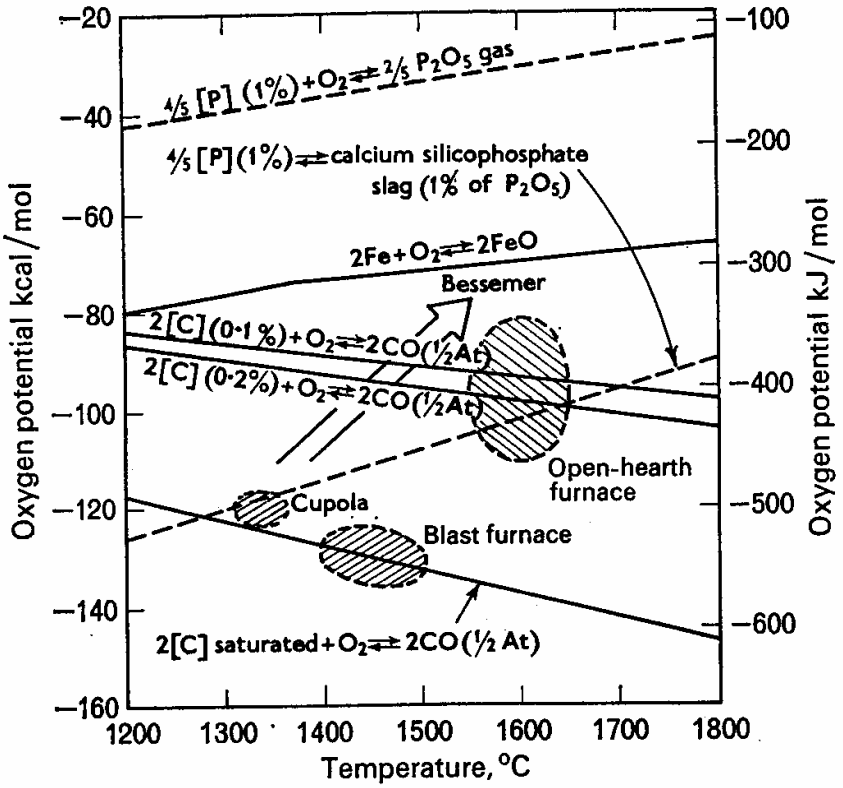

Figure 2.2 Comparison of the oxygen potentials at which phosphorus can transfer from the metal to slag with the oxygen potentials of various iron and steel making processes[7]

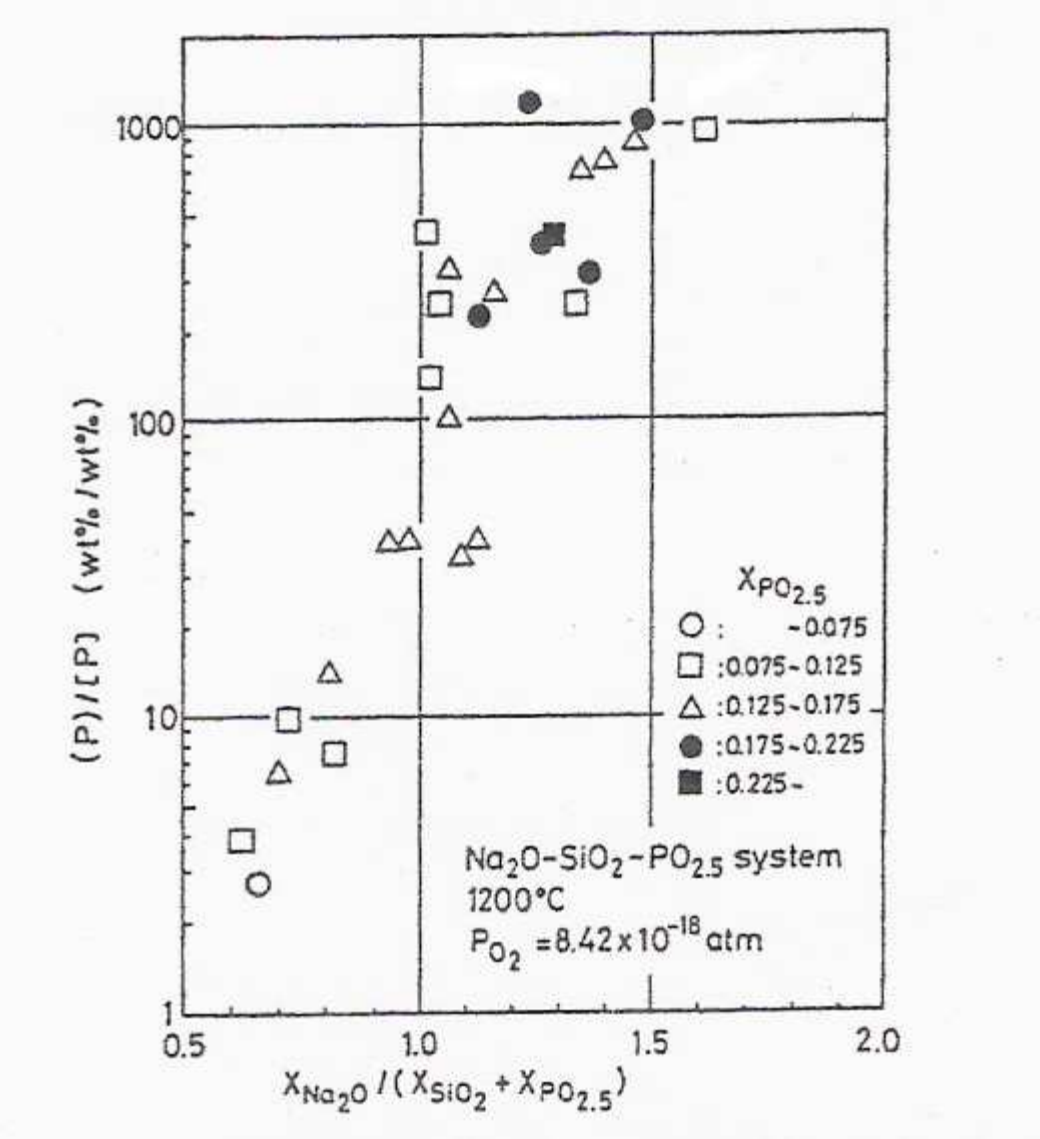

Figure 2.3 The relationship between phosphorus distribution ratio and $X_{Na_2O}/\left(X_{SiO_2}+X_{PO_{2.5}}\right)$ at 1200°C[11]

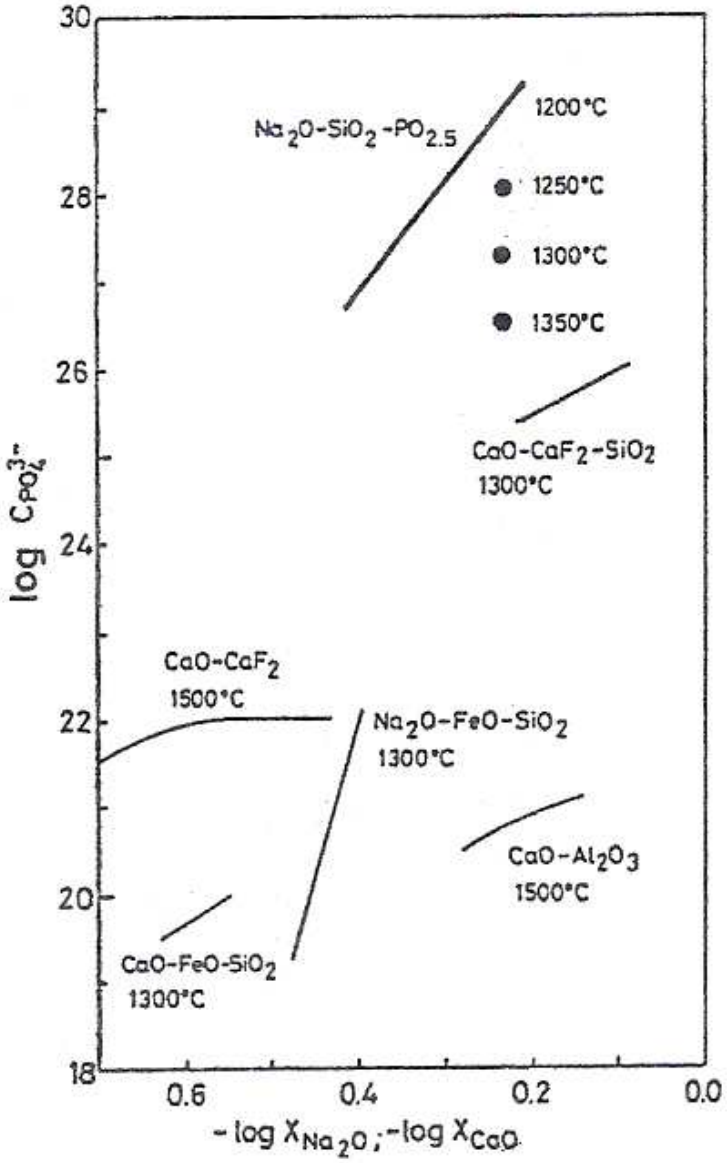

Figure 2.4 A comparison of phosphate capacities of various systems[11]

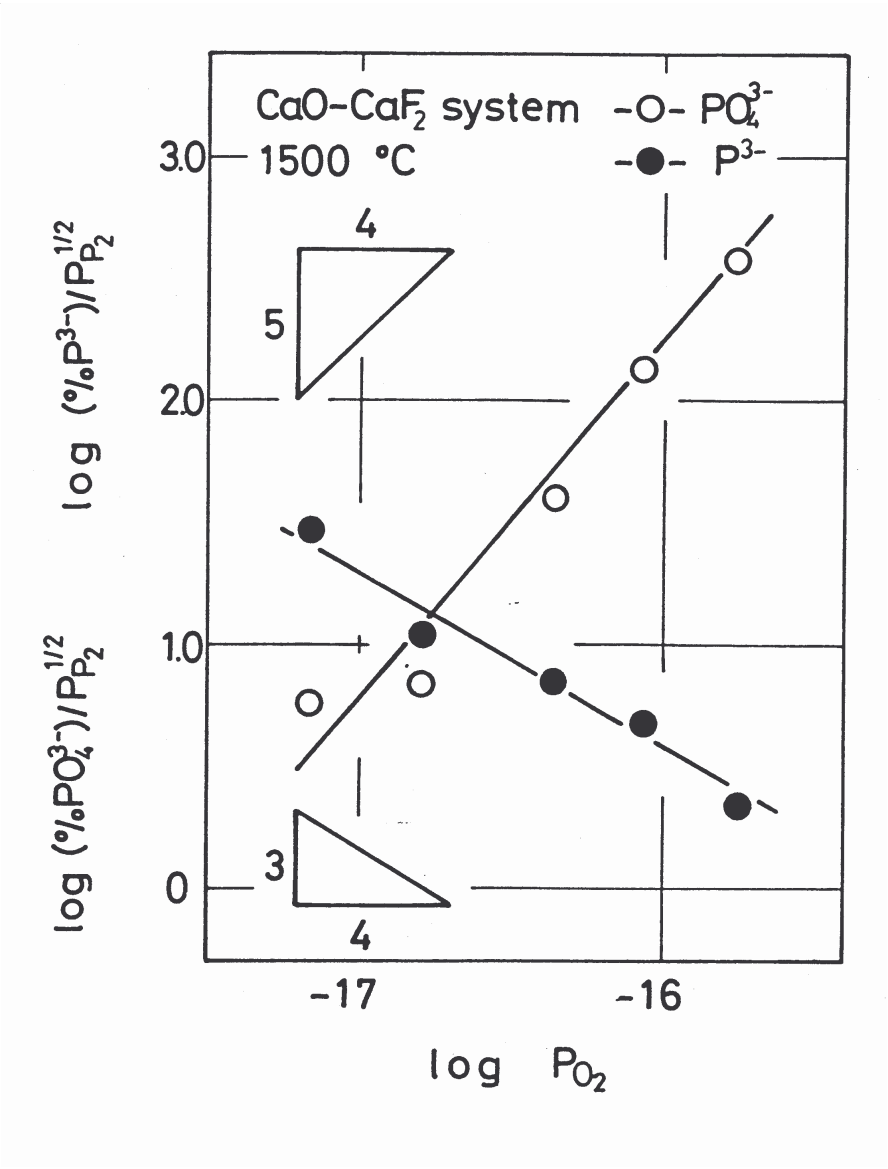

Figure 2.5 $(\%PO_4^{3-})/(P_{P_2}^{1/2})$ and $(\%P^{3-})/(P_{P_2}^{1/2})$ in the $CaO_{(sat)}$-CaF_2 melt as a function of Log Po_2[13]

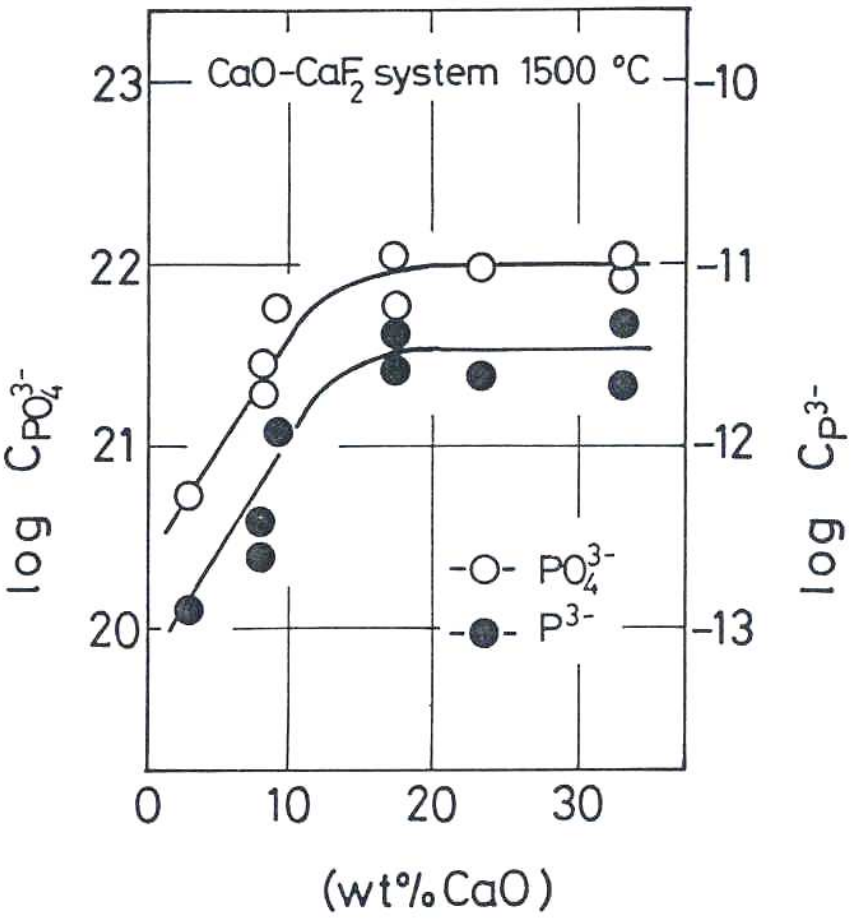

Figure 2.6 Phosphate and phosphide capacities against wt. % CaO for the $CaO\text{-}CaF_2$ system[13]

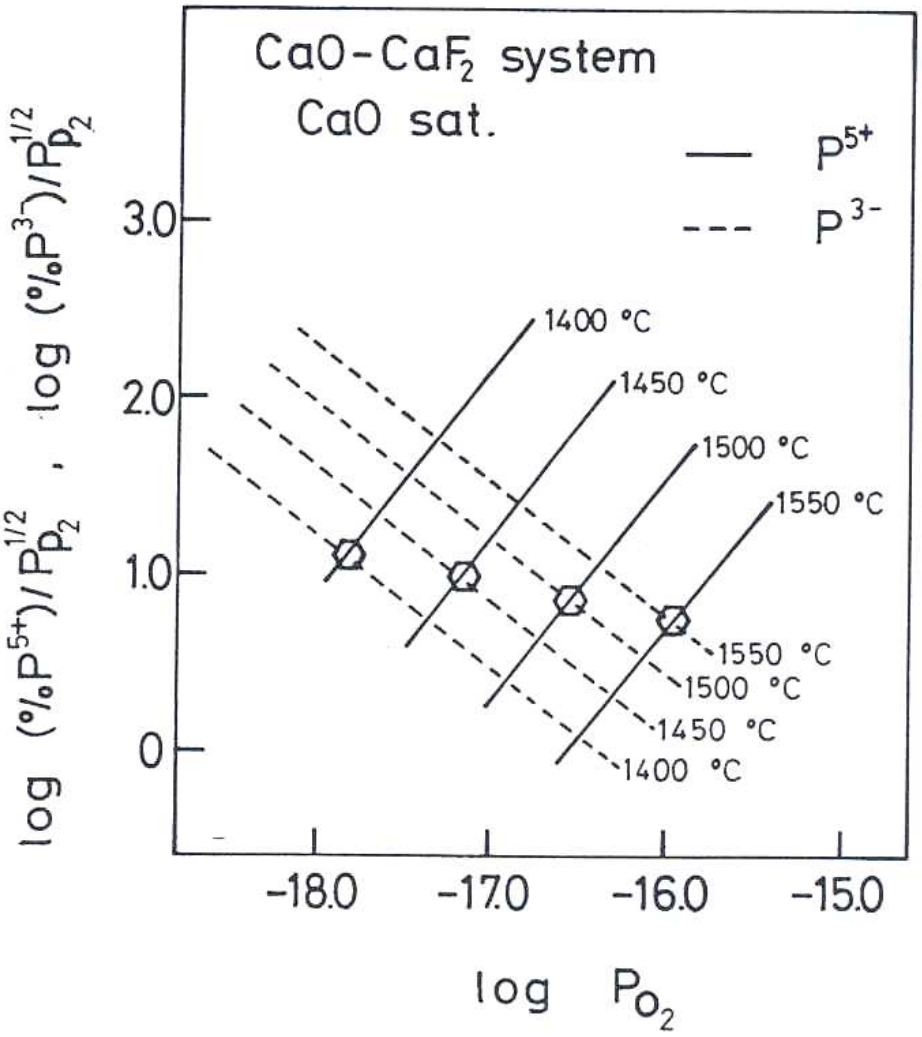

Figure 2.7 Stability of phosphate and phosphide ions for the $CaO-CaF_2$ system saturated with CaO as a function of log Po_2[13]

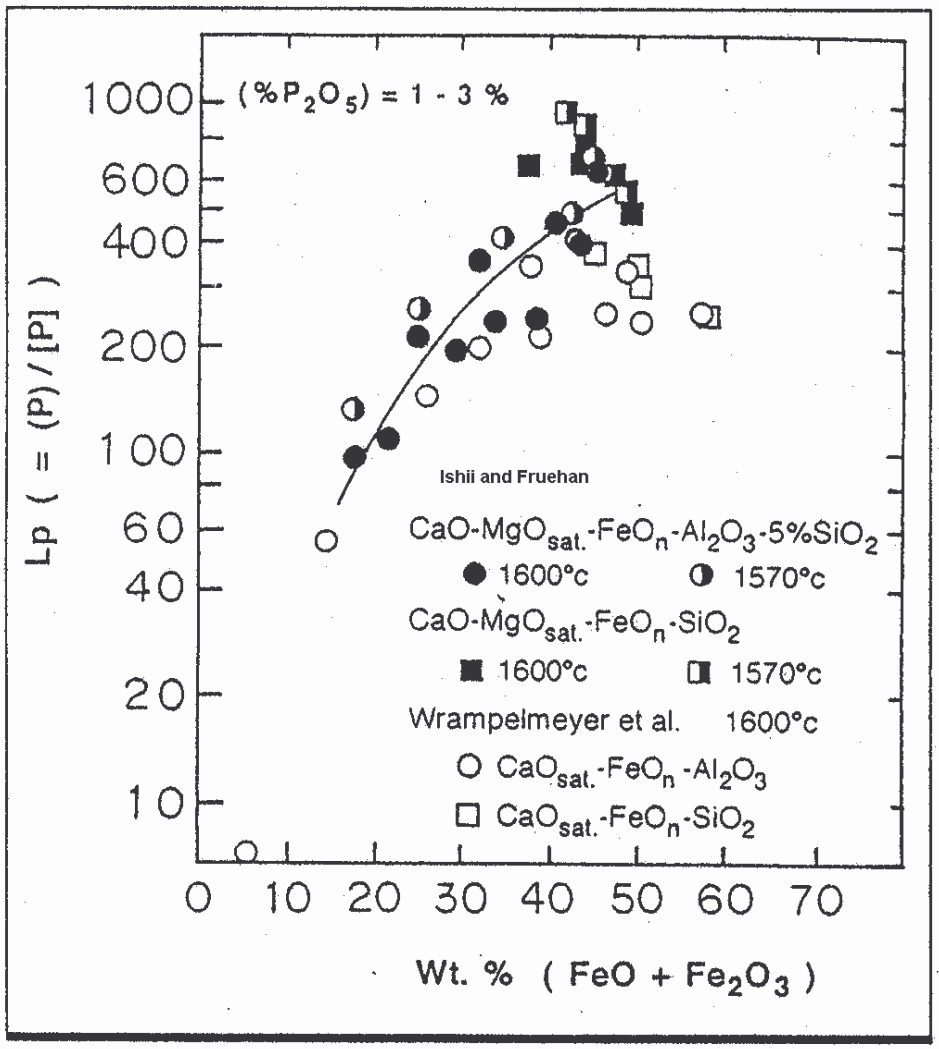

Figure 2.8 Phosphorus distribution ratios as a function of wt. % (FeO_n)[25]

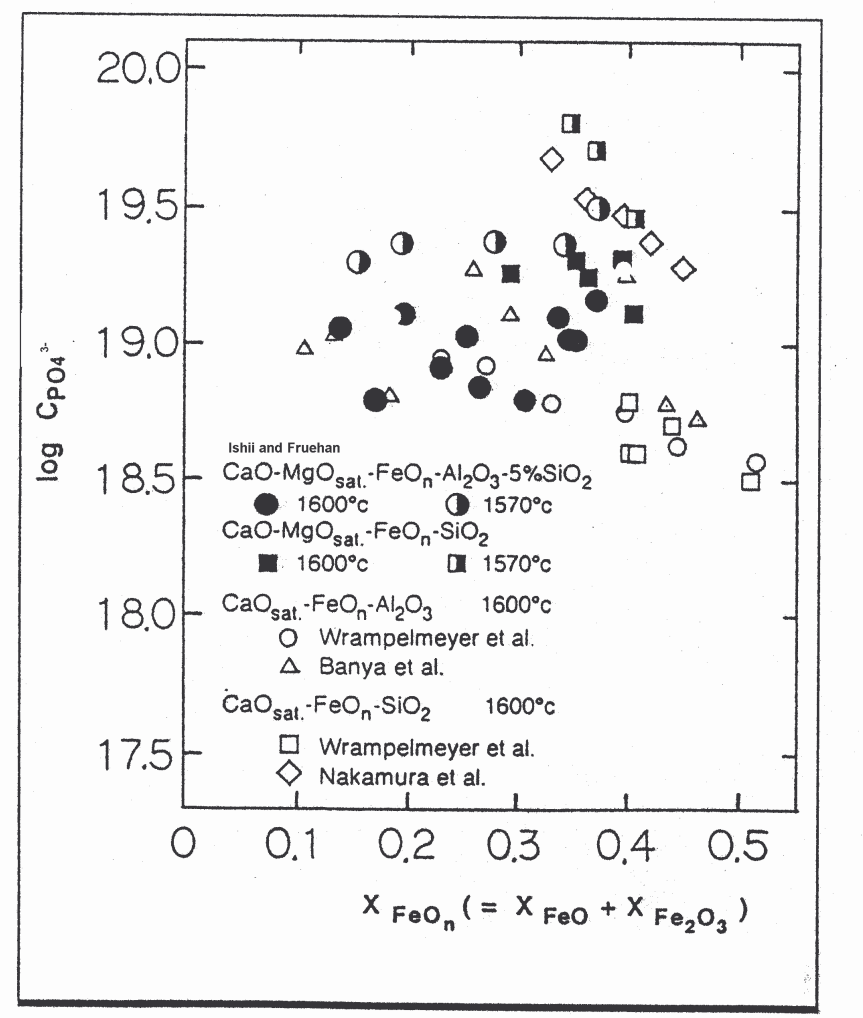

Figure 2.9 The relationship between $(\log C_{PO_4^{3-}})$ and mole fraction of $FeO_n(X_{FeOn})$[25]

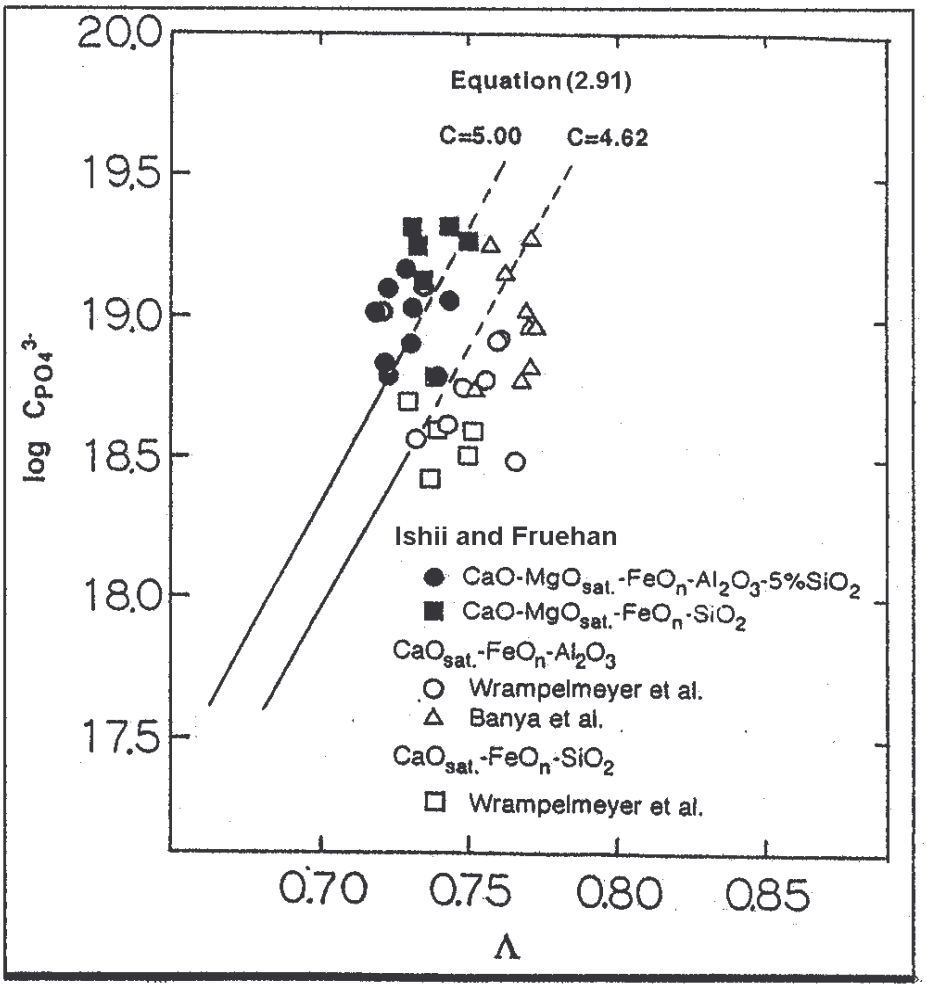

Figure 2.10 Relation between the optical basicity, Λ and $\log C_{PO_4^{3-}}$ for highly basic slags at 1600°C [25]

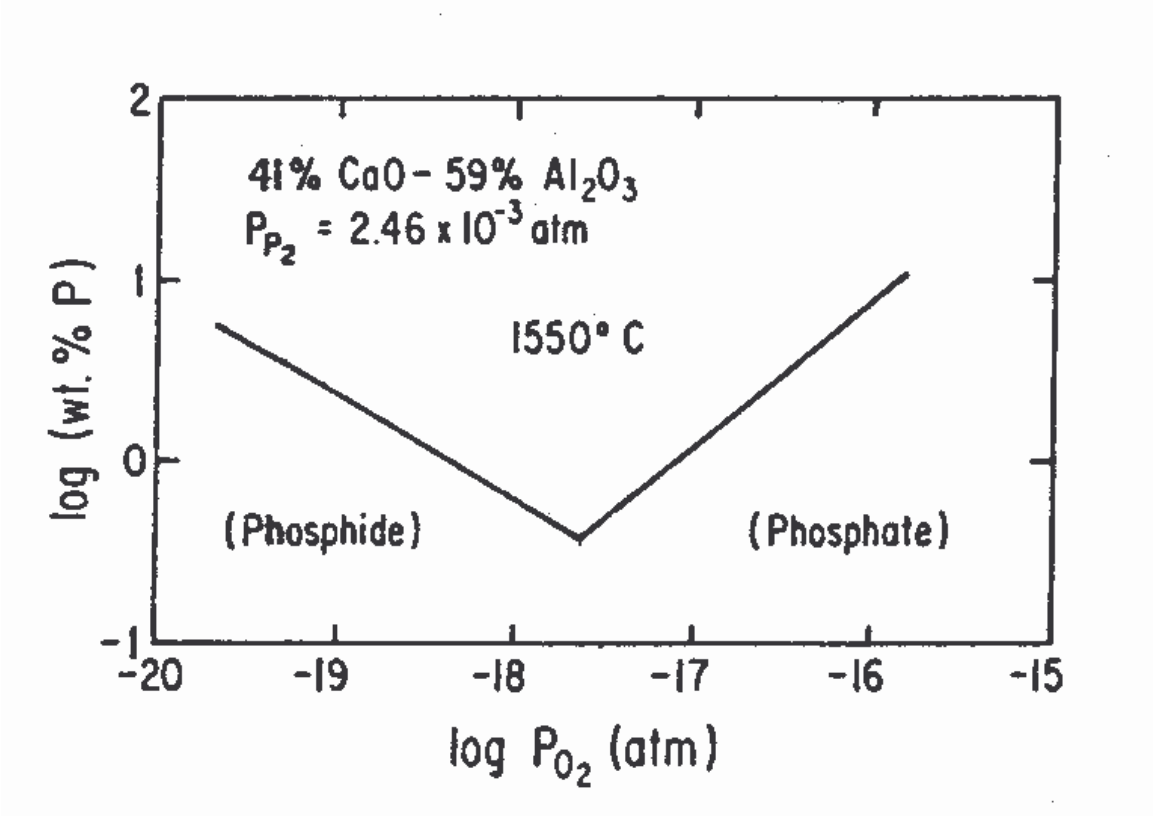

Figure 2.11 Phosphide/ phosphate solubilities in a calcium aluminate slag[12]

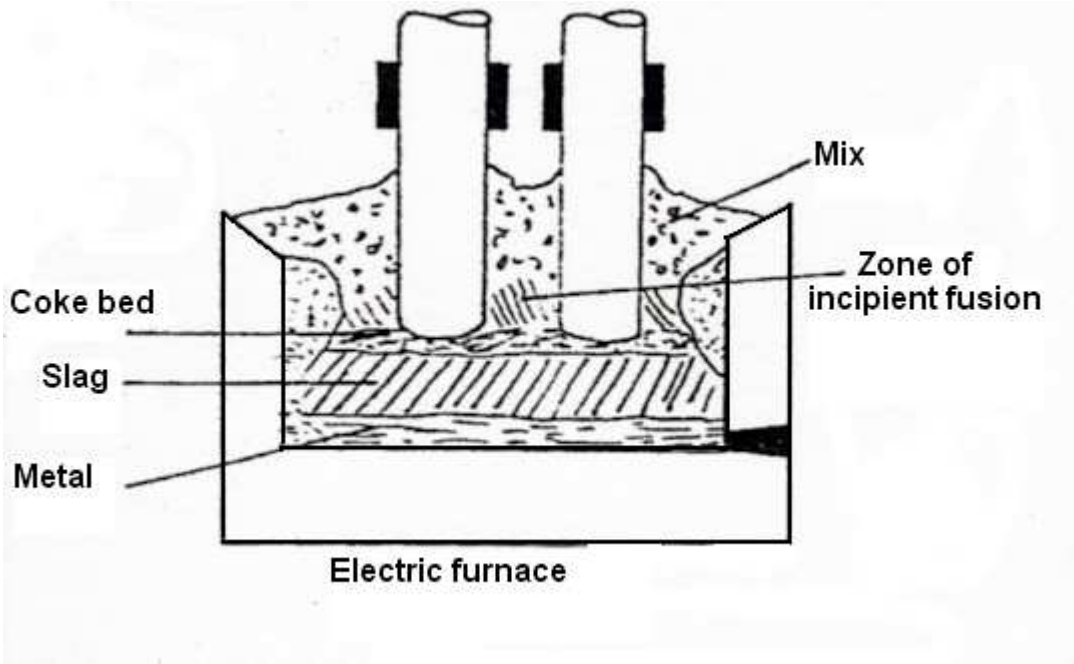

Figure 2.12 Schematic diagram of the electric furnace showing zone of incipient fusion[44]

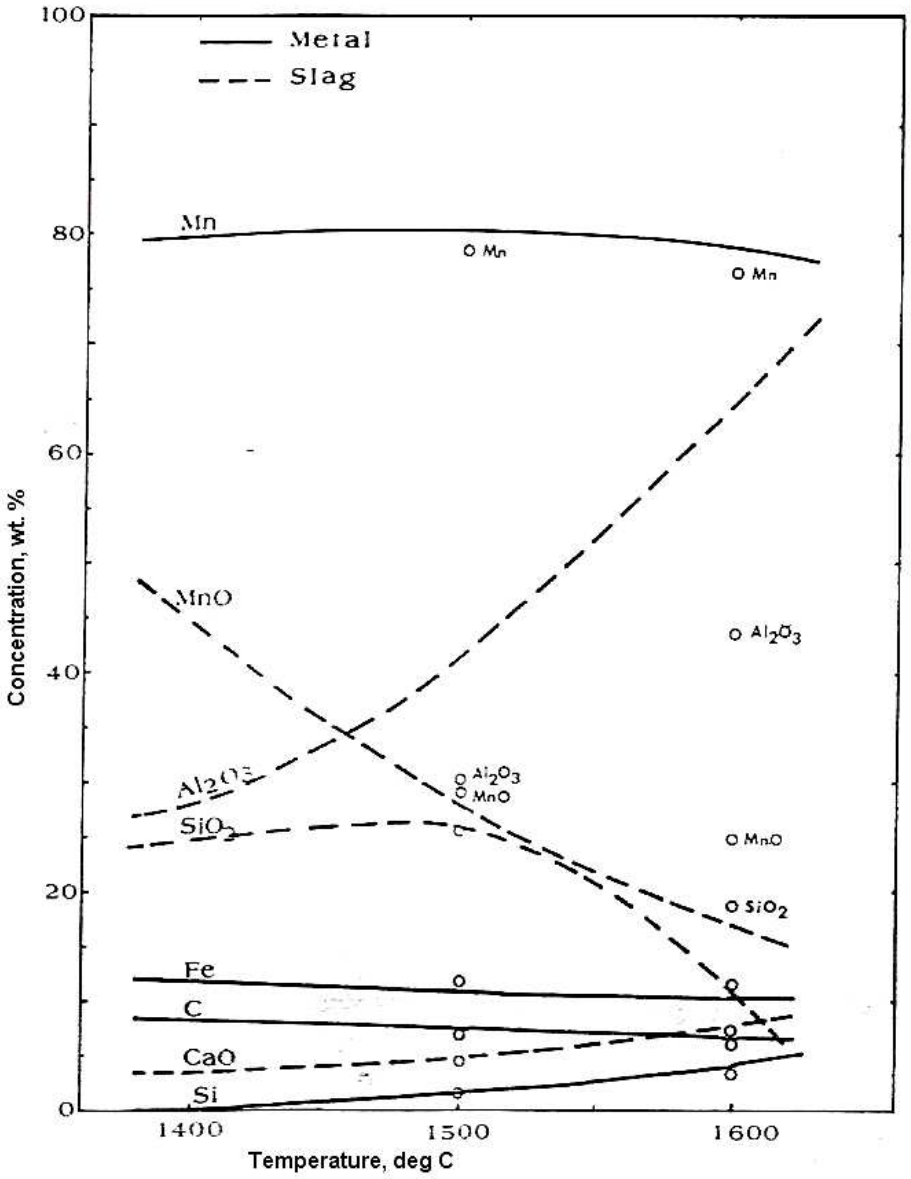

Figure 2.13 Variation of metal and slag composition with temperature at carbon saturation condition[47]

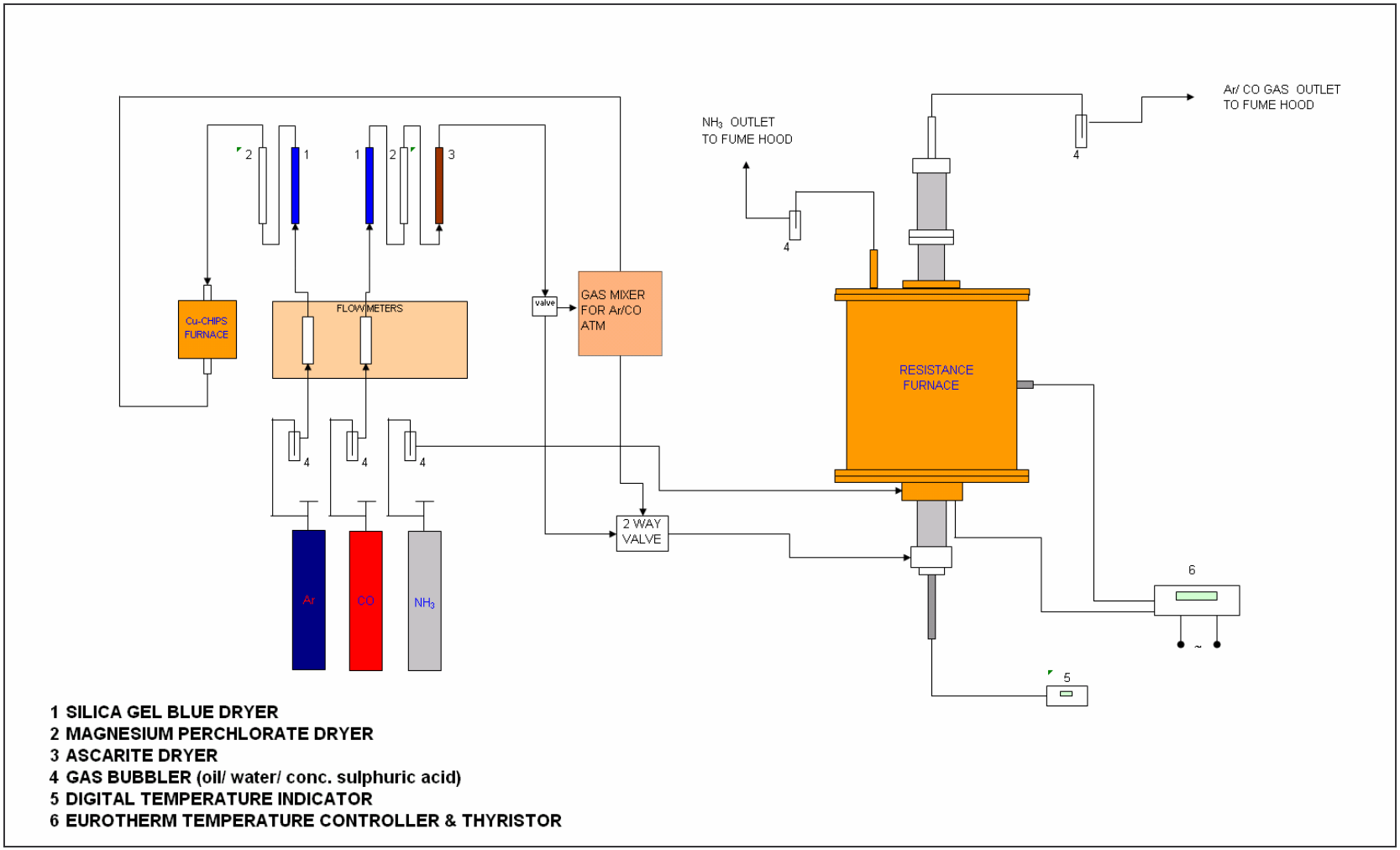

Figure 3.1: Flow diagram of the experimental set-up

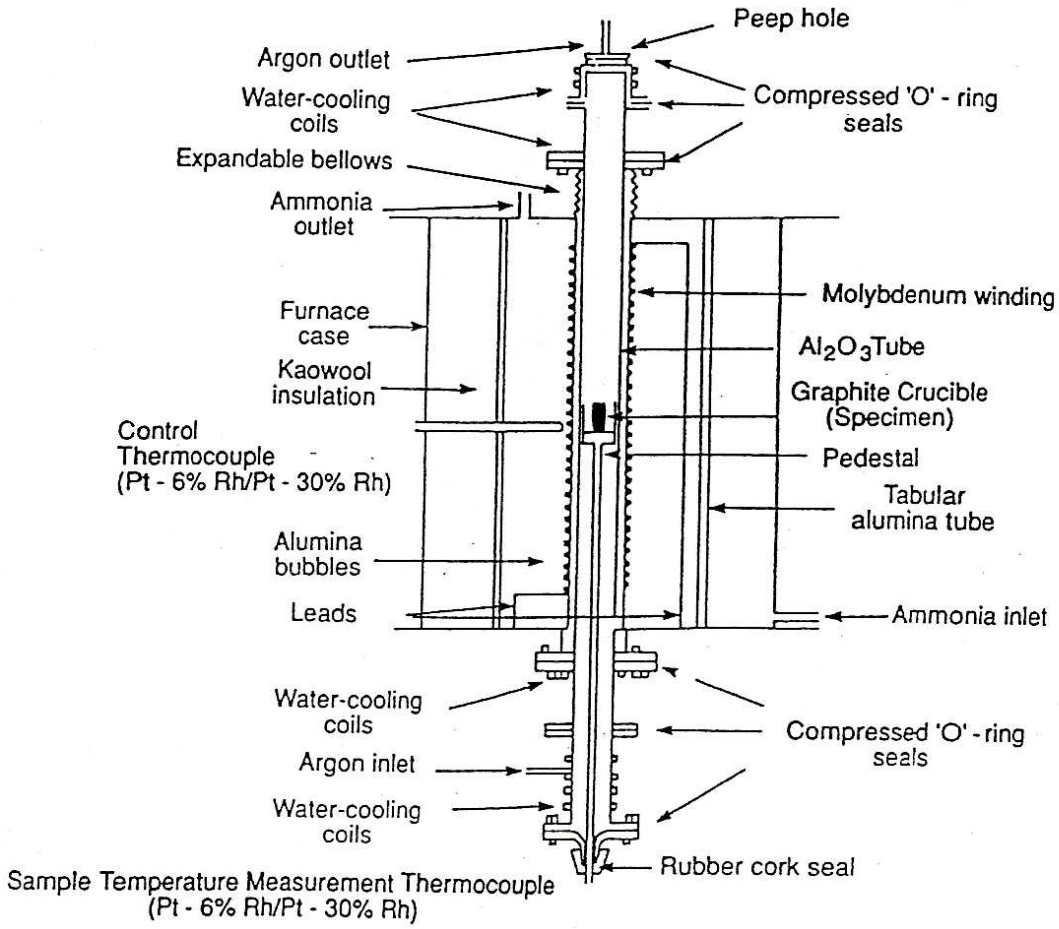

Figure 3.2: A cross section of the vertical molybdenum wound resistance furnace.